5-Methyl-cytosine stabilizes DNA but hinders DNA hybridization revealed by magnetic tweezers and simulations

Xiao-Cong Zhao[1],[†], Hai-Long Dong[2],[†], Xiao-Lu Li[1], Hong-Yu Yang[1], Xue-Feng Chen [1], Liang Dai [3], Wen-Qiang Wu [4], Zhi-Jie Tan [2],*, and Xing-Hua Zhang [1],*

[1]The Institute for Advanced Studies, College of Life Sciences, State Key Laboratory of Virology, Hubei Key Laboratory of Cell Homeostasis, Wuhan University, Wuhan 430072, China, [2]Department of Physics and Key Laboratory of Artificial Micro & Nano-structures of Ministry of Education, School of Physics and Technology, Wuhan University, Wuhan 430072, China, [3]Department of Physics, City University of Hong Kong, Hong Kong 999077, China and [4]School of Life Sciences, State Key Laboratory of Crop Stress Adaptation and Improvement, Key Laboratory of Plant Stress Biology, Henan University, Kaifeng 475001, China

ABSTRACT

5-Methyl-cytosine (5mC) is one of the most important DNA modifications and plays versatile biological roles. It is well known that 5mC stabilizes DNA duplexes. However, it remains unclear how 5mC affects the kinetics of DNA melting and hybridization. Here, we studied the kinetics of unzipping and rezipping using a 502-bp DNA hairpin by single-molecule magnetic tweezers. Under constant loading rates, 5mC increases the unzipping force but counterintuitively decreases the rezipping force at various salt and temperature conditions. Under constant forces, the non-methylated DNA hops between metastable states during unzipping and rezipping, which implies low energy barriers. Surprisingly, the 5mC DNA can't rezip after fully unzipping unless much lower forces are applied, where it rezips stochastically in a one-step manner, which implies 5mC kinetically hinders DNA hybridization and high energy barriers in DNA hybridization. All-atom molecular dynamics simulations reveal that the 5mC kinetically hinders DNA hybridization due to steric effects rather than electrostatic effects caused by the additional methyl groups of cytosines. Considering the possible high speed of DNA unzipping and zipping during replication and transcription, our findings provide new insights into the biological roles of 5mC.

INTRODUCTION

Methylation is the most important modification of DNA and one of the most important epigenetic mechanisms governing fundamental cellular processes across species (1,2). In bacteria, 5-methyl-cytosine (5mC), *N*-4-methyl-cytosine (4mC) and *N*-6-methyl-adenine (6mA) occur at specific targets, which play critical roles in modulating DNA-protein interactions, chromosome replication, DNA mismatch repair, gene transcription and formation of epigenetic phenotypes (2). In eukaryotes, 5mC is the most frequent DNA methylation. In plants, 5mC often occurs at CpG dinucleotides as well as CHG and CHH elements (where H = A, T or C). In mammals including humans, most 5mC occurs at CpG sites and a new 5mC is established by transferring the methyl group (CH3) to cytosine by DNA methyltransferases DNMT3A and DNMT3B (3). The 5mC can be erased through an active demethylation pathway involving three sequential steps of the oxidation of 5mC to 5-hydroxymethylcytosine (5hmC), to 5-formylcytosine (5fC) and then to 5-carboxylcytosine (5caC) by TETs enzymes, followed by base excision and base excision repair to convert the abasic site back to non-methylated cytosines (4).

Single-molecule techniques have been widely used to explore the effects of 5mC on various aspects of DNA. Besides the traditional bisulfite sequencing to map 5mC, the polymerase kinetics (5) and nanopore (6,7) have been used to directly detect 5mC besides sequencing DNA at the single-molecule level. Single-molecule manipulation and fluorescence experiments have showed that CpG methylation increased the stability of nucleosomes (8–11) and the tighter wrapping of DNA might hinder the accessibility of

*To whom correspondence should be addressed. Tel: +86 15827632615; Fax: +86 02768753780; Email: zhxh@whu.edu.cn
Correspondence may also be addressed to Zhi-Jie Tan. Tel: +86 15827627809; Fax: +86 02768752569; Email: zjtan@whu.edu.cn
†The authors wish it to be known that, in their opinion, the first two authors should be regarded as Joint First Authors.

transcription-related proteins such as RNA polymerase II ([12]). Single-molecule fluorescence experiments and molecular dynamics (MD) simulations revealed that the additional CH3 on cytosines could relocate the high-valent cations from major grooves of DNA to interhelical regions, thereby increasing DNA–DNA attraction ([13,14]). By equilibrium measurements using magnetic tweezers (MT), we revealed that 5mC promoted high-valent-cation-induced DNA condensation through enhancing DNA–DNA attraction ([15]). The effects of 5mC on the bendability of DNA have been widely studied by single-molecule techniques for years but are still unclear. Recently, Zaichuk et. al measured the force–extension curves of a ∼6000-bp DNA using MT experiments and reported that 5mC increased the overall bendability of the long DNA ([16]). Yeou *et al.* applied bending force on a 30-bp short DNA using a D-shaped nanostructure in single-molecule fluorescence experiments and found a profound mechanism that the location of 5mC and the bending force determined the local bendability of DNA through affected the formation of kinks, which might contribute to the stability of the nucleosome structure ([17]). These two important recent works imply that how 5mC affects the bendability of DNA is still a complicated problem.

Melting is one of the most important processes of double-stranded DNA (dsDNA) that occurs during replication and transcription. It is well known that 5mC generally stabilizes dsDNA in heat-induced melting experiments indicated by the increase in melting temperature of dsDNA ([18–20]). Thus, methylation-sensitive high-resolution melting measurement has been widely used to assess the level of 5mC of DNA collected from cells ([21]). *In vivo*, 5mC can reduce the speed to separate the two strands in dsDNA by helicase and polymerase ([19]). Besides heat and molecule motors, ds-DNA can also be ruptured by force. Single-molecule manipulation experiments have revealed that 5mC stabilized ds-DNA in force-induced melting experiments indicated by the increase of shearing peeling force of short dsDNA ([22,23]).

Despite extensive studies on how 5mC affects the stability of dsDNA, the effects of 5mC on the kinetics of DNA melting and hybridization as well as the mechanisms are still unclear. Single-molecule manipulation techniques, such as MT and optical tweezers have been widely used to obtain the time-courses during unzipping and rezipping of long DNA hairpins near the equilibrium, which exhibited multiple intermediate states due to the sequence-depended energy barriers ([24–29]). In this work, we aim to characterize the effects of 5mC on the kinetics of DNA melting and hybridization using MT experiments. Then, we will perform all-atomic MD simulations to reveal the molecular mechanisms of the effects of 5mC.

MATERIALS AND METHODS

Magnetic tweezers

We have used our home-built MT to study the elasticities of DNA and RNA and described the MT in our recent works ([15,30–32]). As shown in Supplementary Figure S1, we built the MT using an inverted microscope (IX73, Olympus) equipped with a 100× oil immersion objective (PlanSAPO NA1.3, Olympus), on top of which a flow cell was placed. We controlled the vertical position of the objective by a

Piezo objective scanner (P-721, Physik Instrumente). We fixed a pair of vertically aligned neodymium magnets (5 mm cubes) separated by a 1 mm gap in a holder to attract the paramagnetic beads and exert constant forces on the DNA. We used the L-509 motor (Physik Instrumente) to control the vertical position of the magnets to control the stretching force on the DNA. We illuminated the field of view with a red collimated LED-light source through the magnets gap. We imaged the beads using a CCD camera at 100 frames per second (MER2-230-168U3M, Daheng Imaging) and calculated the three-dimension positions of the beads following the previously proposed algorithm ([33]). We settled the MT in an ultra-clean room with a constant temperature of 22°C and used Bioptechs Objective Heater System to wrap around the oil objective to control the temperature in the flow cell.

Flow cell

We cleaned both the larger (24 × 72 mm) and smaller (24 × 50 mm) cover slides with piranha solution in a staining jar, functionalized the larger slides with 3-aminopropylsilane (ATPES, Sigma-Aldrich), and assembled each flow cell with a larger slide, a smaller slide and double-side taps (Supplementary Figure S1). We used a syringe (needle inner diameter of 2 mm) to draw the inlet and outlet of the flow cell with room temperature vulcanized silicone rubber (KE445, Shinetsu). After the rubber dried, we attached polystyrene microbeads (3 μm in diameter, Spherotech) to the internal surface of the flow cell by nonspecific adsorption and used the polystyrene beads as reference beads to remove the drift during long-time MT measurements.

One day before each MT experiment, we coated the APTES-functionalized slide with sulfo-SMCC (Thermo Fisher Scientific) in the flow cell, anchored the thiol end of DNA to the slide and passivated the surfaces overnight using 1% bovine serum albumin (Sigma-Aldrich) and 1 mM dithiothreitol (Sigma-Aldrich) in phosphate-buffered saline. Then, we attached a streptavidin-coated paramagnetic bead (2.8 μm in diameter, Dynabeads M-270) to the biotin end of the DNA. To increase the precision of force, we determined the relationship between the position of the magnets and the magnetic force exerted on DNA for each bead as we previously described ([34]). We performed all MT measurements at 1 mM Tris–HCl, pH 7.5 supplemented with various concentrations of NaCl and MgCl$_2$.

DNA hairpin sample

We prepared the DNA hairpin sample containing a TTTT loop and a 502-bp stem. By PCR, we prepared the 5mC DNA (all cytosines were methylated) using 5-methyl-dCTP (New England Biolabs) and prepared the non-Me DNA (none cytosines were methylated) using dCTP supplemented with dATP, dTTP and dGTP. As shown in Figure 1A, we amplified four DNA segments by PCR (step i), digested them with BsaI-HF (New England Biolabs) to generate 4-nt stick ends (step ii) and ligated them together using T4 DNA ligase (New England Biolabs, step iii). Then, we used Terminal transferase (New England Biolabs) to transfer biotin-11-dUTP (Roche) to the 3' ends of the DNA (step
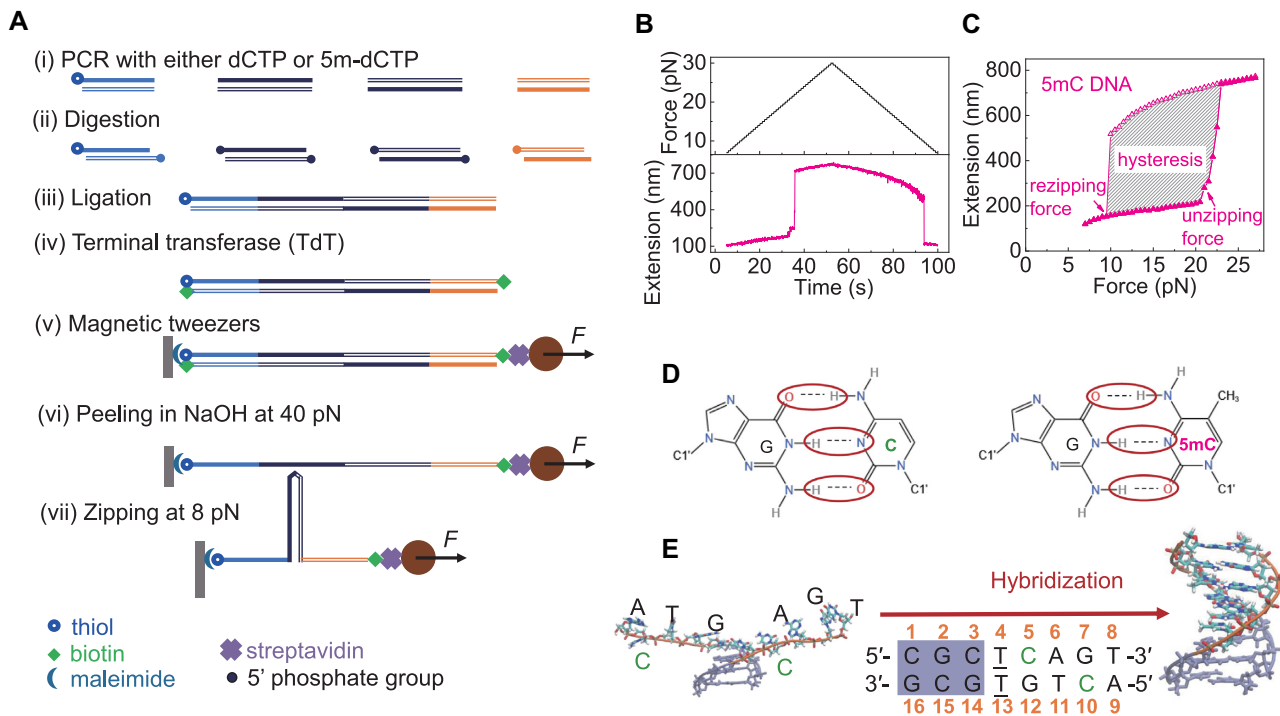
Figure 1. Methods of MT experiments and MD simulations. (**A**) Preparation of the 502-bp DNA hairpin sample for MT experiments. (**B**, **C**) Measurement of unzipping force, rezipping force and hysteresis in an unzipping-rezipping cycle. This representative measurement was performed at 150 mM NaCl and 22°C using 5mC DNA. The DNA hairpin was stretched through a force-cycle containing a force-increasing scan and a force-decreasing scan, during which the extension in DNA was recorded in panel B. The determined unzipping force (upward arrow), rezipping force (downward arrow), and hysteresis (shadowed area) were donated in panel C. (**D**) Illustration for Watson–Crick C–G and 5mC–G base pairs in MD simulations. The atom pairs in red circles were used to calculate the average H-bond distance between H and O (or N) atom pairs in the analyses. (**E**) The initial unfolded structure and the final folded structure in the MD simulations. The 16 nucleotides were numbered (orange). The shadowed segment indicated the three fixed base pairs. The T–T mismatch was underlined. Three were two cytosines (number 5 and 10, olive) initially at the unfolded state.

iv). We anchored the dsDNA for the MT experiment and peeled off the untethered single-stranded DNA (ssDNA) strand in the dsDNA at 100 mM NaOH and 40 pN (steps v-vi). Because DNA segments 2 and 3 contained complementary sequences, the long DNA hairpin rezipped at 8 pN when we changed the buffer into 1 mM Tris–HCl pH 7.5 and 150 mM NaCl (step vii). Please find the step-by-step protocols to prepare the DNA hairpin sample and the sequences of oligos used in Sec1 of the supplementary data.

Measurements of unzipping force, rezipping force and hysteresis

We illustrated the method we determined unzipping force, rezipping force and hysteresis in unzipping-rezipping cycles in a representative experiment using 5mC DNA at 150 mM NaCl and 22°C (Figure 1B, C). As shown in Figure 1B, we stretched the DNA hairpin through a force-cycle containing a force-increasing scan (0.5 pN/s) through a set of constant forces where the hairpin unzipped, followed by a force-decreasing scan (-0.5 pN/s) through the same set of constant forces where the hairpin rezipped. At each constant force, we held the DNA for one second during which we calculated the average in the extension of DNA. As shown in Figure 1C, each force-cycle yielded an unzipping force–extension curve (filled squares) and a rezipping force–extension curve (empty squares). We determined the unzipping force to be the lowest force where an abrupt increase in

extension occurred in the unzipping force–extension curve (upward arrow). Similarly, we determined the rezipping force to be the highest force where an abrupt decrease in extension occurred in the rezipping force–extension curve (downward arrow). We calculated the level of hysteresis to be the area between the unzipping and rezipping force–extension curves to evaluate the speed of DNA unzipping and rezipping (shadowed area). For each molecule at each salt and temperature condition, we repeated the force-cycles three times and used at least four independent molecules to obtain the averages and standard deviations of the unzipping force, rezipping force and hysteresis.

All-atom MD simulations

To understand the effects of 5mC on the kinetics of DNA hybridization, we performed all-atom MD simulations for a DNA duplex with and without 5mC (Figure 1D). We used an 8-bp dsDNA with the sequence of 5′-CGCTCAGT-3′/5′-ACTGTGCG-3′ containing a T–T mismatch (underlined). To reduce the conformational space, we permanently fixed the first three base pairs CGC/GCG in the base-paired state while initially setting the last four base pairs CAGT/ACTG in the unfolded state (Figure 1E). We arranged a T–T mismatch to avoid the possible influence of the three fixed base pairs on the hybridization of the last four base pairs. Note that the last four bases for hybridization cover all four kinds of nucleobases.

We obtained the initial unfolded state for the hybridization as follows. Firstly, we built a B-form DNA by the nucleic acid builder (NAB) (35), Afterward, two constant forces of 50 pN in two opposite directions were applied to phosphate groups in T and A at the end of dsDNA while fixing the first three CG base pairs in the steered MD simulation. Ultimately, we randomly selected an unfolded state with the last four base pairs completely dissociated (Figure 1E). For 5mC DNA, we replaced a hydrogen atom on the C5 atom of each cytosine with CH3 (Figure 1D).

Starting from the initial unfolded structures of the non-Me DNA and 5mC DNA, we performed the MD simulations using the Gromacs 4.6 software package (36) with a recently refined AMBER ff99bsc1 force field (35,37) and TIP3P water model (38). The charges for the methylated cytosines were obtained from the restrained electrostatic potentials method (RESP) for the QM calculations with the Gaussian09 simulation package by Carvalho *et al.* (39) following the conventional AMBER charge derivation methodology (40). In each simulation, we placed the DNA and water molecules in a cubic box of size $10 \times 10 \times 10$ nm^3. We added 104 Na$^+$ and 90 Cl$^-$ ions with the model from Joung and Cheatham to ensure the bulk salt of 150 mM NaCl (41–44), and we added 66 Mg^{2+}, 92 Na$^+$ and 210 Cl$^-$ with the Åquist model for Mg^{2+} based on our previously proposed method to ensure another typical bulk salt of 150 mM NaCl and 100 mM Mg^{2+} (30,32,42). We employed periodic boundary conditions along with the particle mesh Ewald (PME) summation method for the Coulomb interactions (45) and used a smooth cut-off of 10 Å for the van der Waals energy. We used an integration step of 2 fs in conjunction with the leap-frog algorithm (46). The systems were energy minimized for 5000 steps, and then were heated to 298 K and equilibrated with the Nosé–Hoover temperature coupling until 0.1 ns under isothermal-isochoric ensemble (NVT) conditions (47). Afterward, we conducted the 0.1 ns equilibrations under isothermal-isobaric ensemble (NPT) conditions with Parrinello-Rahman pressure coupling (48). In NVT and NPT simulations, we restrained the nucleic acids by a harmonic potential with a force constant of 1000 kJ/mol·nm^{-2}. Finally, we continued five independent MD simulations for either non-Me DNA or 5mC DNA in the NPT ensemble (time-step 2 fs, $P = 1$ atm, $T = 298$ K). Please see our previous works for even more details of the MD simulations (32,49–51).

RESULTS

The effects of 5mC on unzipping-rezipping cycles of long DNA hairpin at various salt and temperature conditions.

We first studied the effects of 5mC on unzipping-rezipping cycles at various NaCl concentrations at 22°C (Figure 2A–D). At both the low NaCl concentration of 10 mM (Figure 2A) and the high NaCl concentration of 500 mM (Figure 2B), 5mC increased the unzipping force. Counterintuitively, 5mC decreased the rezipping force, which was conflicting with the known effects that 5mC stabilizes dsDNA. In the broad range of 10 mM to 500 mM NaCl, 5mC increased the unzipping force of DNA by $\sim$2.5 pN but dramatically decreased the rezipping force by $\sim$7.0 pN (Figure 2C). The difference between the rezipping and unzipping forces was

$\sim$0.5 pN for the non-Me DNA but increased to $\sim$10.2 pN for the 5mC DNA (Figure 2C). In line with these results, 5mC increased the hysteresis in the unzipping and rezipping cycles by over 6-fold (Figure 2D). We found the hysteresis in the unzipping-rezipping cycle decreased with the concentration of NaCl, which could be explained by the effects that the Na$^+$ cations neutralized the negative charges of ssDNA, reduced electrostatic repulsion and helped the two strands of ssDNA come into proximity with each other (52,53).

We fitted the unzipping force, rezipping force and hysteresis as linear functions of log([NaCl]/1 M). We found that 5mC had no significant effects on the slopes for the unzipping force (both slopes for non-Me DNA and 5mC DNA were $\sim$4.7 pN) and slight effects on the slopes for the rezipping force ($\sim$4.8 pN for non-Me DNA and $\sim$4.9 for 5mC DNA). As shown in Figure 2D, the hysteresis decreased with the increase of log([NaCl]/1 M). The slopes were -62 pN·nm for non-Me DNA and –121 pN·nm for 5mC DNA.

As Mg^{2+} is a critical divalent ion in cells, we also studied the effects of 5mC at various MgCl$_2$ concentrations at a physiological background monosalt concentration of 150 mM NaCl at 22°C (Figure 2E–H). As shown in the representative unzipping-rezipping curves at 2 (Figure 2E) and 100 mM (Figure 2F) MgCl$_2$, 5mC increased the unzipping force but counterintuitively decreased the rezipping force, which was similar to the result obtained in NaCl solutions without MgCl$_2$ (Figure 2A, B). We fitted the unzipping force, rezipping force and hysteresis as linear functions of log([MgCl$_2$]/1 M). We found while had minor effects on the slopes for unzipping force (1.4 pN for non-Me DNA and 1.3 pN for 5mC DNA), 5mC significantly increased the slopes for rezipping force from 1.4 pN for non-Me DNA to 1.8 pN for 5mC DNA (Figure 2G). As shown in Figure 2H, the hysteresis decreased relatively faster with the increase of log([MgCl$_2$]/1 M) for 5mC DNA (slope of -348 pN·nm) than for non-Me DNA (slope of –49 pN·nm), which implied the effects of 5mC on the hysteresis were weaker at high MgCl$_2$ concentrations.

Taking advantage of our MT with temperature control, we also measured the effects of 5mC at various temperatures at 150 mM NaCl (Figure 2I–L). As shown in the representative unzipping-rezipping curves at 22°C (Figure 2I) and 36°C (Figure 2J), 5mC increased the unzipping force but decreased the rezipping force also. We fitted the unzipping force, rezipping force and hysteresis as linear functions of temperature (Figure 2K, L). As shown in Figure 2K, while had minor effects on the slopes for unzipping force (–0.24 pN/°C for non-Me DNA and –0.23 pN/°C for 5mC DNA), 5mC remarkably changed the slopes for rezipping force from –0.22 (non-Me DNA) to –0.09 (5mC DNA) pN/°C. We found the hysteresis in the unzipping-rezipping cycle decreased at higher temperatures, which could be explained by higher thermal energy enabling strands to better overcome the energy barrier posed by the repulsive electrostatic forces between two negatively charged ssDNA strands (54). The slopes of hysteresis were –6.9 pN·nm/°C for non-Me DNA and –55.2 pN·nm/°C for 5mC DNA (Figure 2L).

To determine whether the results at 0.5 pN/s shown in Figure 2A–L were independent of the load rate, we repeated these measurements using a lower loading rate of 0.2 pN/s and a higher loading rate of 1 pN/s at various NaCl con-
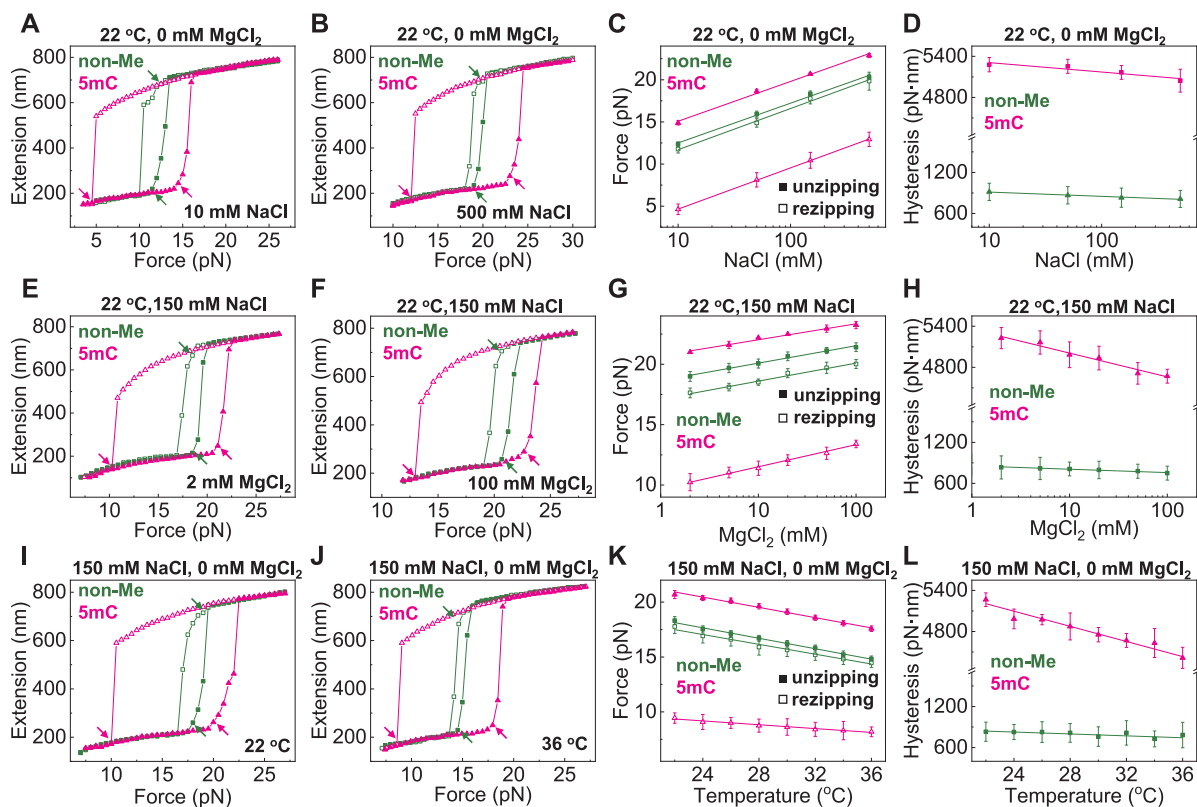
Figure 2. The effects of 5mC on the unzipping-rezipping cycle of long DNA hairpin at various NaCl concentrations (A–D), MgCl$_2$ concentrations (E–H) and temperatures (I–L). (**A**, **B**, **E**, **F**, **I**, **J**) Representative unzipping (filled squares) and rezipping (empty squares) force–extension curves. The determined unzipping and rezipping forces were marked as upward and downward arrows, respectively. (**C**, **G**, **K**) The effects of 5mC on unzipping (filled squares) and rezipping (empty squares) forces. The error bars were the standard deviations obtained from four molecules. We fitted the forces as linear functions of log([NaCl]/1 M), log([MgCl$_2$]/1 M) or temperature, respectively. (**D**, **H**, **L**) The effects of 5mC on hysteresis in the unzipping-rezipping cycle. The error bars were the standard deviations obtained from four molecules. We fitted the hysteresis as linear functions of log([NaCl]/1 M), log([MgCl$_2$]/1 M) or temperature, respectively.

centrations, MgCl$_2$ concentrations and temperatures (Supplementary Figure S2 and S3). We found the effects of 5mC on unzipping force, rezipping force and hysteresis were consistent with the results at 0.5 pN/s. At the loading rates of 0.2 pN/s and 1 pN/s, 5mC increased the unzipping force but counterintuitively decreased the rezipping force at each buffer condition. Also, the level of hysteresis decreased at higher salt concentrations and higher temperatures.

The effects of 5mC on DNA unzipping and rezipping at constant forces

Previous single-molecule experiments have demonstrated that the time-courses of DNA unzipping under constant forces showed multiple intermedia states due to the sequence-dependent energy barriers (24–29). Based on these works, we studied the effects of 5mC on the time-courses of DNA unzipping at 150 mM NaCl and 22°C under constant forces (Figure 3A, B). As shown in Figure 3A, after we elevated the applied force from 5.0 pN to 18.0 pN and held the force at 18.0 pN, the non-Me DNA unzipped through multiple intermediate metastable states, which was consistent with previous results (24–29). Using the 10 nearest-neighbor (NN) base-pair energies ob-

tained in force-induced DNA unzipping experiments by optical tweezers (25), we plotted the free energy landscape as a function of the location of the unzipping fork near the equilibrium force (Supplementary Figure S4). When we plotted the extension histograms from four molecules together and compared them with the free energy landscape, we found the locations of long-lived intermedia states during unzipping were in line with the local minimums in the energy landscape, which verified the intermedia states were due to the sequence-dependent energy barriers.

As shown in the enlarged views of Figure 3A, the non-Me DNA hopped between metastable states both at the beginning and end of DNA unzipping, which implied the DNA unzipped near the equilibrium. As shown in Figure 3B, after we elevated the force from 5.0 to 20.0 pN and held it at 20.0 pN (higher than 18.0 pN for non-Me DNA), the 5mC DNA unzipped through multiple intermediate metastable states as well. We did not compare the locations of intermediate states with the free energy landscape because of the lacking of NN base-pair energies for 5mC DNA under force. As shown in the enlarged views, the 5mC DNA hopped between metastable states at the beginning of DNA unzipping but couldn't rezip after being fully unzipped. We repeated
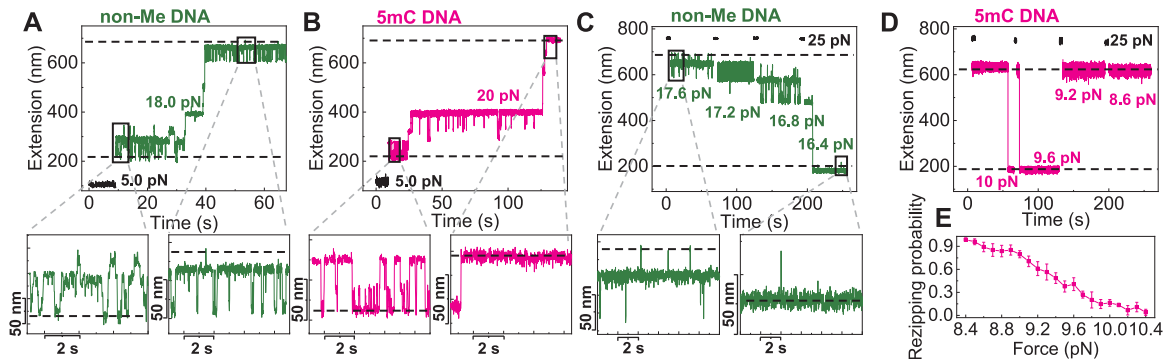
Figure 3. The effects of 5mC on the time-courses of DNA unzipping and rezipping at constant forces at 150 mM NaCl and 22°C. The beginning and end of unzipping/rezipping were enlarged for clarity. The extensions of fully zipped and unzipped DNA were marked as dashed horizontal lines. (**A**) Unzipping of non-Me DNA. (**B**) Unzipping of 5mC DNA. (**C**) Rezipping of non-Me DNA. (**D**) Rezipping of 5mC DNA. (**E**) The probability of rezipping for 5mC DNA as a function of applied force. The error bars were the standard deviations obtained from four molecules.

the DNA constant-force unzipping experiments using four molecules for each of non-Me DNA and 5mC DNA and obtained consistent time-courses (Supplementary Figure S5).

After the DNA hairpin fully unzipping at the high force of 25.0 pN, we dropped to lower forces to study the time-courses of DNA rezipping at 150 mM NaCl and 22°C under constant forces (Figure 3C, D). We found the non-Me DNA rezipped at constant forces in the range of 17.6–16.4 pN (Figure 3C), hopping between metastable states both at the beginning and end of rezipping. However, 5mC DNA rezipped at the constant forces in the range of 10.0–8.6 pN (much lower than the rezipping forces for non-Me DNA) in a one-step manner (Figure 3D). During the 60-second holding time of each constant force, whether 5mC DNA might rezip or not showed a strong stochastic phenomenon. The 5mC DNA might rezip at the higher force of 10.0 pN but might not rezip at the lower force of 8.6 pN (Figure 3D). We performed the rezipping experiments at each constant force 25 times for each 5mC DNA molecule in the range of 8.4–10.4 pN. At each constant force, the experiments using four molecules yielded the average and error bar in the probability of DNA rezipping (number of rezipping events divided by number of total events) which showed strong stochastics (Figure 3E). For 5mC DNA, the much lower rezipping force and the stochastic one-step rezipping time-courses were in line with a picture that 5mC caused a high kinetic barrier in rezipping after fully unzipped, and the 5mC DNA required much lower rezipping forces to overcome the barrier. Once overcome the kinetic barrier, the 5mC DNA rezipped fast due to the low forces far from the equilibrium and 5mC stabilized dsDNA. We repeated the DNA constant-force rezipping experiments using four molecules for each of non-Me DNA and 5mC DNA and obtained consistent time-courses (Supplementary Figure S6).

In hysteresis measurements, we found the effects of 5mC were weaker at higher concentrations of MgCl$_2$ (Figure 2H) and higher temperatures (Figure 2L). The hysteresis in the unzipping and rezipping cycle of 5mC DNA decreased from ∼5265 pN·nm at 150 mM NaCl and 22°C to ∼3948 pN·nm at 100 mM MgCl$_2$ and 36°C (Supplementary Figure S7). To test whether 5mC still hinders DNA hybridization at 150 mM NaCl, 100 mM MgCl$_2$ and 36°C, we repeated the constant-force DNA unzipping and rezipping

experiments at this salt and temperature condition (Supplementary Figure S8). We obtained similarly unzipping time-courses (Supplementary Figure S8A, B). The non-Me DNA hopped between metastable states at both the beginning and end of unzipping. The 5mC DNA hopped between metastable states at the beginning but couldn't rezip after fully rezipped. We also obtained similar rezipping time-courses (Supplementary Figure S8C, D). The non-Me DNA hopped between metastable states while the 5mC DNA rezipped in a one-step manner at much lower forces. For 5mC DNA, we performed rezipping experiments at each constant force 25 times for each molecule (four molecules in all) in the range of 12.8–14.9 pN and calculated the probability of DNA rezipping which showed strong stochastics (Supplementary Figure S8E). Thus, 5mC also hindered DNA hybridization at this high salt and high temperature condition.

To verify the effects of 5mC on DNA unzipping and rezipping under constant forces (Figure 3 and Supplementary Figures S5, S6 and S8) were not caused by the accidental specific DNA sequence, we performed the constant-force experiments using another 502-bp DNA sequence and obtained similarly unzipping/rezipping time-courses (Supplementary Figures S9 and S10). For this new DNA sequence, the non-Me DNA hopped between multiple metastable states during unzipping and rezipping. The 5mC DNA, however, couldn't rezip after fully unzipping unless much lower forces were applied where it rezipped stochastically in a one-step manner.

MD simulations reveal that 5mC slows down DNA hybridization

To understand the mechanism of why 5mC hinders DNA hybridization, we performed all-atom MD simulations. First, we performed five independent MD simulations and calculated the mean hybridization time which was defined as the mean time when the H-bond distances all reached within 3 Å for non-Me DNA and 5mC DNA, respectively (Figure 4A). The hybridization time of 5mC DNA (230 ± 85 ns) was significantly longer than that of non-Me DNA (72 ± 31 ns). This result showed a similar trend to the MT measurements, suggesting that our simulations repro-
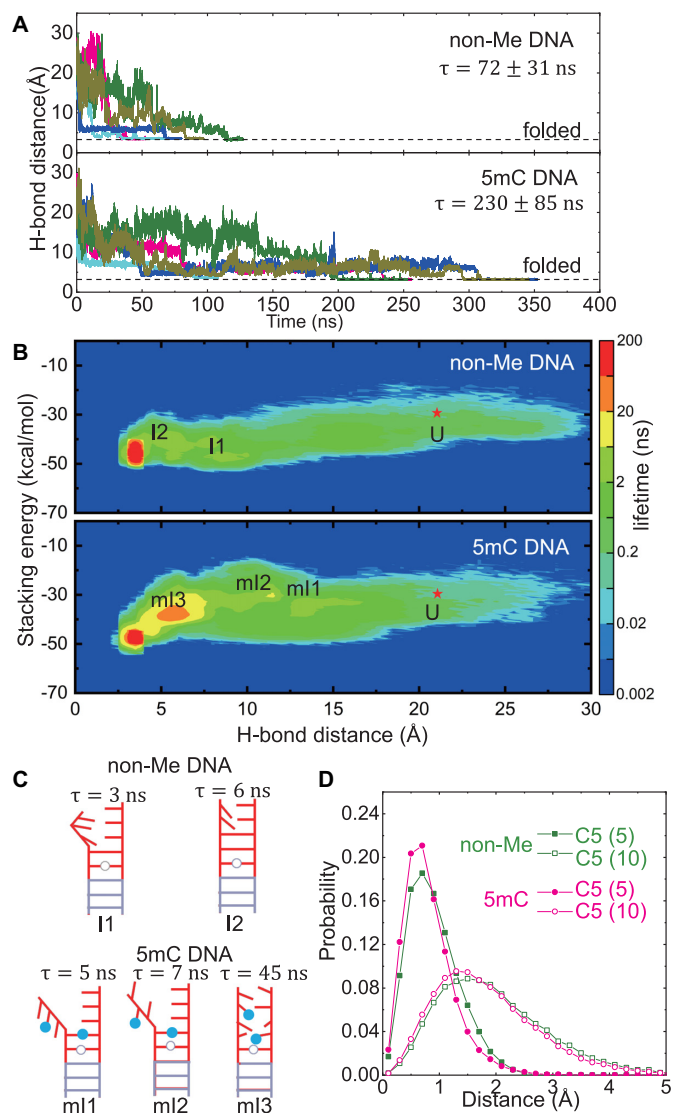
Figure 4. The 5mC slowed down DNA hybridization revealed by MD simulations. (**A**) The average H-bond distance as a function of the MD simulation time from five independent MD trajectories. The dash lines donated the H-bond distance of the folded state. The average and standard deviation of the time to fold (τ) obtained from five independent MD trajectories were donated. (**B**) The lifetime landscapes of different states versus H-bond distance and stacking energy. Here, the H-bond distance and stacking energy were the average values for the last four base pairs. The bins used in our calculations were 0.5 Å for the H-bond distance and 0.5 kcal/mol for the stacking energy. The stars denote the initial unfolded structure and red regions denoted the folded state. Here, U stood for the initial unfolded state with H-bond distance of ~21 Å for non-Me DNA and 5mc DNA; I1 and I2 stood for the intermediate states with the H-bond distances of ~8 Å and ~5 Å for non-Me DNA; mI1, mI2, and mI3 stood for the intermediate states with the H-bond distances of ~13, ~11 and ~6 Å for 5mc DNA. (**C**) The lifetimes and the sketch structures for different intermediate states during hybridization. Here, the filled circles denoted the additional CH3 and the empty circles denoted the T–T mismatches. (**D**) The normalized probability of the distances of C5 atoms of cytosines (olive) and methylated cytosines (magenta) from their respective equilibrium positions in the folded states. The cytosines numbered 5 and 10 were defined in (**B**).

duced the experimental results that 5mC kinetically hindered DNA hybridization.

To reveal why 5mC slows down DNA hybridization, we built the lifetime landscapes of different states including the initial unfolded state, partially folded intermediate states and the folded states. To build a lifetime landscape, we employed two coordinates: one was the average distance between the H-bond atomic pairs of the last four base pairs per base pair (Figure 1E), and the other was the stacking energy of the last four base pairs (22,55,56). Here, we calculated the stacking energy using the AMBER package (22) according to Ref (57). Note that the H-bond distance was ~21 Å for the initial unfolded state and ~3.1 Å for the ultimate folded state.

As shown in Figure 4B, compared with non-Me DNA, the hybridization process of 5mC DNA involved intermediate states which had long lifetimes, especially the mI3 state with the H-bond distance of ~5.5 Å and the stacking energy of ~–35 kcal/mol. The long-lived intermediate states in the hybridization process of 5mC DNA slowed down DNA hybridization. Next, we examined the structures to explore why these intermediate states during the hybridization of 5mC DNA have long lifetimes. As shown in Figure 4C, the long-lived intermediate structures of 5mC DNA generally had less formed base pairs and fewer single-strand self-stacks around the methylated cytosines, especially for mI2 and mI3, which had very close H-bond distances to the folded state with visibly disordered base stacks. This result suggested that the 5mC would lead to long-lived intermediate states close to the folded state in the H-bond length while such state had visibly disordered stacks around the methylated cytosines.

Why did 5mC bring the intermediate states with visibly disordered stacks and a long lifetime? First, we analyzed the effect of 5mC on C–G base pairing. As illustrated in Figure 4B, CH3 should not affect the C–G base-pairing since CH3 was beside the base-pairing interface and H atoms in CH3 had only too low positive charges (~0.1e for H atom in CH3) to form a hydrogen bond with highly negatively charged O and N atoms. Second, we analyzed the change in local atom-charge distribution due to 5mC. We found that the H atom bonded to the C5 atom replaced by CH3 slightly decreased the charge of the group of C5 and its bonded atoms from –0.3 e to –0.2 e, i.e. the total charge of C5 and H atoms was ~–0.3 e for cytosine and that of C5 and CH3 atoms was ~–0.2 e. Thus, 5mC did not bring significant change in the local charge of the C5-bonded group. Third, we analyzed the change in local atom excluded volume due to 5mC. We found that the H atom bonded to C5 with a radius of 1.46 Å was replaced by the CH3 group with a large effective radius (the summation of the radii of C and H atoms in CH3 is about 3.37 Å), suggesting a stronger excluded volume effect caused by the 5mC. Fourth, we examined the position fluctuation of C5 atoms of cytosines for non-Me DNA and 5mC DNA in a folded state and found that C5 atoms of methylated cytosines were suppressed more strongly than those of non-methylated cytosines (Figure 4D). Therefore, based on the above analyses, the slowed DNA hybridization of 5mC DNA may be mainly caused by the increased excluded volume effect due to the additional CH3.
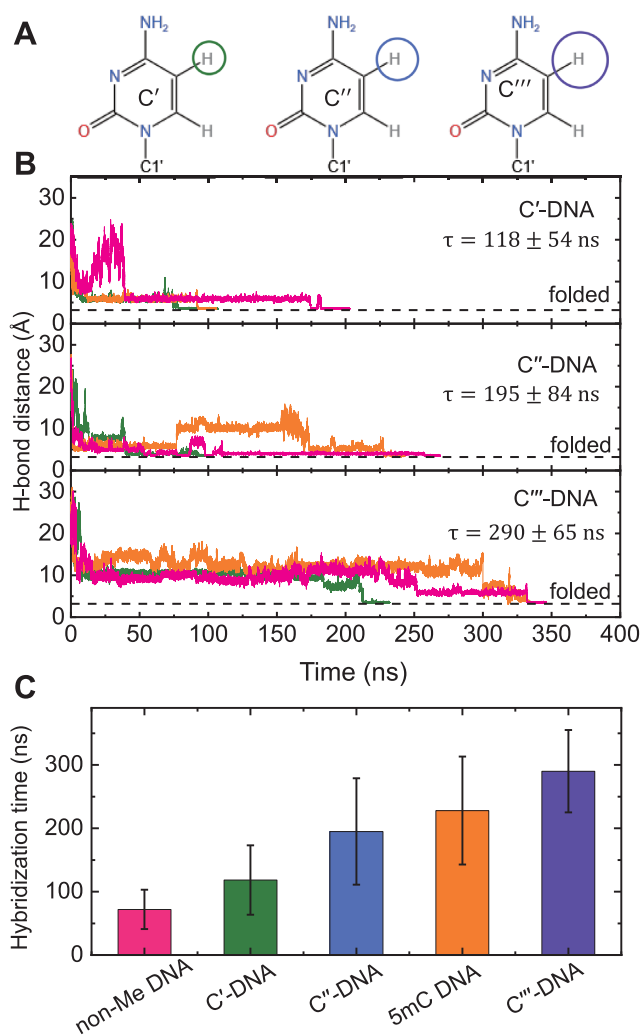
Figure 5. Larger 'H' atoms on the C5 atoms of cytosines slowed down DNA hybridization revealed by MD simulations. (**A**) Illustration of artificial cytosines with 'H' atoms whose radii were adjustable. The radii of artificial atoms increased from the left to the right. (**B**) The average H-bond distance as a function of the simulation time starting from the unfolded state for the hybridization of three model DNAs with three artificial cytosines, respectively. Three independent MD trajectories for each model DNA were donated in different colors. The dashed line was the H-bond distance at the folded state. (**C**) The hybridization time for non-Me DNA, 5mC DNA, and three model DNAs with artificial cytosines. The error bars denoted the standard deviations obtained from three different MD trajectories.

Larger 'H' atoms on C5 of cytosine slow down DNA hybridization revealed by MD simulations

To verify the above-proposed effect of excluded volume of CH3 on DNA hybridization, we designed a model DNA system to perform additional MD simulations. In the model DNA system, each H atom bonded to C5 atoms in cytosines was replaced by an artificial 'H' atom with a larger radius, and the charge of the artificial 'H' atom was kept the same as that of the H atom (Figure 5A). Namely, the model DNA system was completely the same as non-Me DNA including atom charge distribution, only except for the adjustable radius of the 'H' atom bonded to C5 in cytosines. Thus, this model DNA system could not only help to verify the ex-

cluded volume effect of the CH3 but also distinguish the effect of atom charges on DNA hybridization. If the increase of the radii of the artificial atoms slowed the model DNA hybridization, the slower hybridization of 5mC DNA would be mainly caused by the excluded volume effect of CH3, otherwise, the atom charge-related electrostatic interactions would play an important role. Specifically, in our all-atom MD simulations for the model system, the van der Waals radii σ of the artificial 'H' atom bonded with the C5 atom in each cytosine were set as 1.91, 3.37 and 3.59Å, respectively, and these values corresponded to the values of σ_C, $\sigma_C+\sigma_H$ and $\sigma_C+(\sigma_C+\sigma_H)/2$, where σ_C (∼1.91 Å) and σ_H (∼1.46 Å) were the van der Waals radii of C atoms and H atoms. Correspondingly, the three model DNAs were named C'-DNA, C''-DNA and C'''-DNA, respectively (Figure 5A).

As shown in Figure 5B, the mean hybridization times of C'-DNA, C''-DNA and C'''-DNA were ∼118, ∼195 and ∼290 ns, i.e. the hybridization times of the model DNAs increased apparently with the increase of radii of the artificial 'H' atoms. This result indicated that the larger excluded volume of the artificial 'H' atoms visibly slowed down the hybridization of model DNAs. Combined with the results of non-Me DNA and 5mC DNA, the hybridization times of the stimulated DNAs generally increased monotonically with the radius of the atom or atom group bonded to C5 in cytosines (Figure 5C). Moreover, the role of atom-charge-related electrostatic interactions was excluded from our all-atom MD simulations for the model DNAs where only the atom exclusion effect was changed and the atom charge distribution was completely kept the same as non-Me DNA. Therefore, it was the steric hindrance of CH3 that played a major role in slowing DNA hybridization rather than the electrostatic effects.

To further confirm electrostatic effects were not the major cause of 5mC kinetically hindering DNA hybridization, we performed MD simulations at a high salt condition of 150 mM NaCl and 100 mM MgCl$_2$ where the electrostatic effects were further reduced by neutralization of the negative charges of DNA (Supplementary Figure S11A). We found that 5mC increased the hybridization time from 69 ± 28 to 208 ± 57 ns, consistent with that 5mC increased the hybridization time from 72 ± 31 to 230 ± 85 ns at 150 mM NaCl (Supplementary Figure S11B). Thus, electrostatic effects were unlikely to be the major cause of 5mC kinetically hindering DNA hybridization.

DISCUSSION

In eukaryotes, 5mC is the most frequent DNA methylation playing versatile biological roles. Despite extensive studies on how 5mC stabilizes dsDNA, the effects of 5mC on the kinetics of DNA melting and hybridization are still unclear. By stretching a 502-bp long DNA hairpin in MT experiments, we characterized the effects of 5mC on the kinetics of DNA unzipping and rezipping at various salt, temperature and force conditions using force-scanning cycles. We found that 5mC increased the unzipping force but counterintuitively decreased the rezipping force. The hysteresis in unzipping-rezipping cycles was increased by over 5-fold at

constant loading rates of ±0.5 pN/S (Figure 2). Furthermore, we measured the effects of 5mC on DNA unzipping under constant forces near the equilibrium and found 5mC increased the equilibrium force by ∼2 pN (Figure 3A-B). As unzipping of each DNA base pair increased the extension for ∼ 1 nm at ∼20 pN, we obtained that 5mC increased the DNA thermal stabilities by ∼2 pN·nm (∼8 k_BT) per base pair, which was consistent with previous thermal melting experiments (18–20).

We believe the increase of hysteresis mainly due to 5mC slows down DNA hybridization rather than DNA melting based on the following experimental results. First, 5mC increased the unzipping force but decreased the rezipping force in unzipping-rezipping cycles (Figures 2C, G and K). The decrease in rezipping force by 5mC was contradictory to the knowledge that 5mC stabilizes dsDNA, which may be caused by 5mC kinetically hindering DNA hybridization. Second, fitting the unzipping force and rezipping force as linear functions of log([MgCl$_2$]/1 M) and temperature, 5mC DNA and non-Me DNA had similar slopes for unzipping force but had significantly different slopes for rezipping force (Figure 2G and K). Third, in the unzipping-rezipping cycles, the standard deviations of rezipping forces for 5mC DNA were remarkably larger than that for non-Me DNA (Figures 2C, G and K), which implied that 5mC raised the barrier in DNA hybridization and thus made DNA hybridization more stochastic. Fourth, under constant forces, the 5mC DNA couldn't rezip after fully unzipped (Figure 3B) unless a much lower force was applied where it rezipped stochastically in a one-step manner (Figure 3D). The much lower rezipping force and the one-step rezipping manner of 5mC DNA could be explained by that 5mC kinetically hindered the nucleation of a dsDNA segment from the unfolded ssDNA, thus much lower forces were required to accelerate the speed of nucleation. Once the initial dsDNA nucleus formed at these much lower forces, 5mC DNA rezipped very fast exhibiting the one-step manner.

We explored the underlying mechanism of why 5mC slowed down DNA hybridization by MD simulations at 150 mM NaCl. First, we reproduced the experimental results that the hybridization time of 5mC DNA was significantly longer than that of non-Me DNA (Figure 4A). When we looked into the lifetime landscapes and the structures of intermedia states during DNA hybridization, we found that 5mC led to long-lived intermediate states close to the folded state in the H-bond length while such states had visibly disordered single-stranded stacks around the methylated cytosines (Figure 4B, C). As 5mC does not bring significant changes in C–G base-pairing and the local charge distribution near the methylated cytosine, we supposed that the increased excluded volume effect of the additional CH3 might slow down DNA hybridization. To test our hypothesis of volume effect, we designed several model DNA systems where one H atom bonded to C5 atoms of cytosines was replaced by an 'H' with adjustable radii. We found the hybridization times of the model DNAs increased monotonically with the radii of the adjustable 'H' atoms (Figure 5). Our hypothesis of volume effect rather than electrostatic effect was confirmed by MD simulations at the high salt condition of 150 mM NaCl and 100 mM MgCl$_2$, where the neg-

ative charges of DNA were further neutralized. At this high salt condition, the hybridization time of 5mC DNA was also significantly longer than that of non-Me DNA (Supplementary Figure S11). In summary, through MD simulations on non-Me DNA, 5mC DNA, and several model DNAs, we found that due to the steric hindrance of the additional CH3 of cytosines, it became difficult for bulky methylated bases to correctly stack with their neighbors during hybridization, which would extend the hybridization time of 5mC DNA.

There were both the same and different points between MT experiments and MD simulations. First, the lengths of DNA were different. In MT experiments, we used a 502-bp long hairpin. However, it was technically impossible to simulate such a long hairpin utilizing current computing capability. Thus, we simulated a 4-bp DNA sequence CAGT/ACTG containing all four kinds of nucleotides at each strand. MT experiments showed the nucleation of ∼40 bp rezipped DNA (enlarged view of Figure 3C and Supplementary Figure S12) while MD simulation showed the nucleation of 4-bp rezipped DNA. Second, the time scales were different. Due to the low frame rate of the CCD camera, MT experiments only captured the intermediate states that had lifetimes longer than 0.1 s while MD simulations captured the intermediate states that had lifetimes in the time scale of ns. The MT experiments lasted for hours but MD simulations only lasted for less than one millisecond to observe the kinetics during DNA hybridization. The different time scales could be explained by that longer DNA hairpins required longer times to be hybridized, which was revealed by high-frequency optical tweezers (58). Third, the complementary ssDNA strands were under force in MT experiments while they were free of force in MD simulations. To test whether force would change our results of MD simulations, we performed unzipping and rezipping simulations with force using a 2-bp sequence CA/TG (Supplementary Figure S13). In simulations, we kept the folded DNA hairpin through a set of increasing constant forces where the hairpin unzipped and the unzipping force was recorded. Then, we kept the unfolded DNA hairpin through the same set of decreasing constant forces where the hairpin rezipped and the rezipping force was recorded. Under each constant force, we kept the DNA hairpin for 150 ns. Consistent with MT experiments, we found that 5mC increased the unzipping force but decreased the rezipping force in MD simulations. In all, despite the differences between MT experiments and MD simulations, both methods found 5mC kinetically hindered DNA hybridization and MD simulations revealed 5mC hindered DNA hybridization due to steric effects rather than electrostatic effects caused by the additional CH3 groups.

It is previously revealed that the modifications of DNA not only changed the stabilities of dsDNA but also affected the kinetics of DNA melting and hybridization. Using decameric mixed-sequence oligonucleotides, Sabahi et. al reported that despite stabilized dsDNA, propyl- and methoxyethyl-modification of oligonucleotides slowed down hybridization with its complementary unmodified oligonucleotides, which might be due to high preorganization in these modified oligonucleotides (59). They also reported that positively-charged aminopropyl-modification

stabilized short dsDNA and accelerated DNA hybridization (59). Shi *et al.* and Liu *et al.* revealed that 6mA modification selectively slowed down RNA hybridization while minimally impacting the rate of melting, which was explained by the rapid interchange between Watson–Crick anti-6mA/U or mismatch-like syn-6mA/U base pairs, combined with different syn:anti isomer preferences of 6mA when paired (∼1:100) versus unpaired (∼10:1) (60,61). Sanstead *et al.* reported that 5mC stabilized 10-bp short dsDNA and slightly reduced the energy barrier in heat-induced melting (62). They also reported 5hmC and 5fC destabilized the 10-bp short dsDNA and reduced the barrier in melting.

Shi *et al.* and Liu *et al.* revealed that the effects of 6mA on RNA hybridization and melting were different (60,61). Here, we found the effects of 5mC on DNA hybridization and melting might be different also. Our results that 5mC slows down DNA hybridization are not conflicting with previous results that 5mC slightly reduced the energy barrier in DNA melting (62). The different kinetics of DNA unzipping and rezipping implied different transition pathways. The structure of dsDNA was relatively fixed, and thus unzipping of dsDNA had less long-lived intermediate states. At constant forces, the 502-bp long DNA hairpin could overcome the barriers and fully unzip in about 100 seconds near the equilibrium (Figure 3A, B). However, the structure of ssDNA was relatively flexible and the interactions inside the ssDNA stands could bring barriers to DNA rezipping. At constant forces, the DNA could not overcome the barriers after fully rezipped unless lower forces were applied to speed up rezipping (Figure 3C-D). Our MD simulations also revealed long-lived intermediate states with disordered stacks that slowed down DNA hybridization (Figure 5C). DNA unzipping and rezipping play essential roles during the processes of replication and transcription. It was reported that replication (63) and transcription (64) reached high speeds of ∼50 nt/s. At such high speeds, slowing down DNA hybridization by 5mC may affect replication and transcription, which calls for further systematic studies.

DATA AVAILABILITY

The data underlying this article are available in the article and in its online supplementary material.

SUPPLEMENTARY DATA

Supplementary Data are available at NAR Online.

FUNDING

REFERENCES

1. Schubeler,D. (2015) Function and information content of DNA methylation. *Nature*, **517**, 321–326.
2. Sanchez-Romero,M.A., Cota,I. and Casadesus,J. (2015) DNA methylation in bacteria: from the methyl group to the methylome. *Curr. Opin. Microbiol.*, **25**, 9–16.
3. Law,J.A. and Jacobsen,S.E. (2010) Establishing, maintaining and modifying DNA methylation patterns in plants and animals. *Nat. Rev. Genet.*, **11**, 204–220.
4. Wu,X.J. and Zhang,Y. (2017) TET-mediated active DNA demethylation: mechanism, function and beyond. *Nat. Rev. Genet.*, **18**, 517–534.
5. Flusberg,B.A., Webster,D.R., Lee,J.H., Travers,K.J., Olivares,E.C., Clark,T.A., Korlach,J. and Turner,S.W. (2010) Direct detection of DNA methylation during single-molecule, real-time sequencing. *Nat. Methods*, **7**, 461–465.
6. Simpson,J.T., Workman,R.E., Zuzarte,P.C., David,M., Dursi,L.J. and Timp,W. (2017) Detecting DNA cytosine methylation using nanopore sequencing. *Nat. Methods*, **14**, 407–410.
7. Laszlo,A.H., Derrington,I.M., Brinkerhoff,H., Langford,K.W., Nova,I.C., Samson,J.M., Bartlett,J.J., Pavlenok,M. and Gundlach,J.H. (2013) Detection and mapping of 5-methylcytosine and 5-hydroxymethylcytosine with nanopore mspA. *Proc. Natl. Acad. Sci. U.S.A.*, **110**, 18904–18909.
8. Ngo,T.T.M., Yoo,J., Dai,Q., Zhang,Q., He,C., Aksimentiev,A. and Ha,T. (2016) Effects of cytosine modifications on DNA flexibility and nucleosome mechanical stability. *Nat. Commun.*, **7**, 10813.
9. Ngo,T.T.M., Zhang,Q.C., Zhou,R.B., Yodh,J.G. and Ha,T. (2015) Asymmetric unwrapping of nucleosomes under tension directed by DNA local flexibility. *Cell*, **160**, 1135–1144.
10. Choy,J.S., Wei,S., Lee,J.Y., Tan,S., Chu,S. and Lee,T.H. (2010) DNA methylation increases nucleosome compaction and rigidity. *J. Am. Chem. Soc.*, **132**, 1782–1783.
11. Lee,J.Y. and Lee,T.H. (2012) Effects of DNA methylation on the structure of nucleosomes. *J. Am. Chem. Soc.*, **134**, 173–175.
12. Hodges,C., Bintu,L., Lubkowska,L., Kashlev,M. and Bustamante,C. (2009) Nucleosomal fluctuations govern the transcription dynamics of RNA polymerase iI. *Science*, **325**, 626–628.
13. Yoo,J., Kim,H., Aksimentiev,A. and Ha,T. (2016) Direct evidence for sequence-dependent attraction between double-stranded DNA controlled by methylation. *Nat. Commun.*, **7**, 11045.
14. Kang,H., Yoo,J., Sohn,B.K., Lee,S.W., Lee,H.S., Ma,W., Kee,J.M., Aksimentiev,A. and Kim,H. (2018) Sequence-dependent DNA condensation as a driving force of DNA phase separation. *Nucleic Acids Res.*, **46**, 9401–9413.
15. Yang,Y.J., Dong,H.L., Qiang,X.W., Fu,H., Zhou,E.C., Zhang,C., Yin,L., Chen,X.F., Jia,F.C., Dai,L. *et al.* (2020) Cytosine methylation enhances DNA condensation revealed by equilibrium measurements using magnetic tweezers. *J. Am. Chem. Soc.*, **142**, 9203–9209.
16. Zaichuk,T. and Marko,J.F. (2021) Single-molecule micromanipulation studies of methylated DNA. *Biophys. J.*, **120**, 2148–2155.
17. Yeou,S., Hwang,J., Yi,J., Kim,C., Kim,S.K. and Lee,N.K. (2022) Cytosine methylation regulates DNA bendability depending on the curvature. *Chem. Sci.*, **13**, 7516–7525.
18. Nardo,L., Lamperti,M., Salerno,D., Cassina,V., Missana,N., Bondani,M., Tempestini,A. and Mantegazza,F. (2015) Effects of non-CpG site methylation on DNA thermal stability: a fluorescence study. *Nucleic Acids Res.*, **43**, 10722–10733.
19. Rausch,C., Zhang,P., Casas-Delucchi,C.S., Daiss,J.L., Engel,C., Coster,G., Hastert,F.D., Weber,P. and Cardoso,M.C. (2021) Cytosine base modifications regulate DNA duplex stability and metabolism. *Nucleic Acids Res.*, **49**, 12870–12894.
20. Lopez,C.M.R., Lloyd,A.J., Leonard,K. and Wilkinson,M.J. (2012) Differential effect of three base modifications on DNA thermostability revealed by high resolution melting. *Anal. Chem.*, **84**, 7336–7342.
21. Wojdacz,T.K. and Dobrovic,A. (2007) Methylation-sensitive high resolution melting (MS-HRM): a new approach for sensitive and high-throughput assessment of methylation. *Nucleic Acids Res.*, **35**, e41.
22. Severin,P.M.D., Zou,X.Q., Gaub,H.E. and Schulten,K. (2011) Cytosine methylation alters DNA mechanical properties. *Nucleic Acids Res.*, **39**, 8740–8751.
23. Pongor,C.I., Bianco,P., Ferenczy,G., Kellermayer,R. and Kellermayer,M. (2017) Optical trapping nanometry of hypermethylated CPG-island DNA. *Biophys. J.*, **112**, 512–522.

24. Bockelmann,U., Thomen,P., Essevaz-Roulet,B., Viasnoff,V. and Heslot,F. (2002) Unzipping DNA with optical tweezers: high sequence sensitivity and force flips. *Biophys. J.*, **82**, 1537–1553.

25. Huguet,J.M., Bizarro,C.V., Forns,N., Smith,S.B., Bustamante,C. and Ritort,F. (2010) Single-molecule derivation of salt dependent base-pair free energies in DNA. *Proc. Natl. Acad. Sci. U.S.A.*, **107**, 15431–15436.

26. Danilowicz,C., Kafri,Y., Conroy,R.S., Coljee,V.W., Weeks,J. and Prentiss,M. (2004) Measurement of the phase diagram of DNA unzipping in the temperature-force plane. *Phys. Rev. Lett.*, **93**, 078101.

27. Essevaz-Roulet,B., Bockelmann,U. and Heslot,F. (1997) Mechanical separation of the complementary strands of DNA. *Proc. Natl. Acad. Sci. U.S.A.*, **94**, 11935–11940.

28. Huguet,J.M., Ribezzi-Crivellari,M., Bizarro,C.V. and Ritort,F. (2017) Derivation of nearest-neighbor DNA parameters in magnesium from single molecule experiments. *Nucleic Acids Res.*, **45**, 12921–12931.

29. Hatch,K., Danilowicz,C., Coljee,V. and Prentiss,M. (2007) Measurements of the hysteresis in unzipping and rezipping double-stranded DNA. *Phys. Rev. E Stat. Nonlin. Soft Matter Phys.*, **75**, 051908.

30. Fu,H., Zhang,C., Qiang,X.W., Yang,Y.J., Dai,L., Tan,Z.J. and Zhang,X.H. (2020) Opposite effects of high-valent cations on the elasticities of DNA and RNA duplexes revealed by magnetic tweezers. *Phys. Rev. Lett.*, **124**, 058101.

31. Zhang,C., Tian,F.J., Lu,Y., Yuan,B., Tan,Z.J., Zhang,X.H. and Dai,L. (2022) Twist-diameter coupling drives DNA twist changes with salt and temperature. *Sci. Adv.*, **8**, eabn1384.

32. Qiang,X.W., Zhang,C., Dong,H.L., Tian,F.J., Fu,H., Yang,Y.J., Dai,L., Zhang,X.H. and Tan,Z.J. (2022) Multivalent cations reverse the twist-stretch coupling of RNA. *Phys. Rev. Lett.*, **128**, 108103.

33. Van Loenhout,M.T.J., Kerssemakers,J.W.J., De Vlaminck,I. and Dekker,C. (2012) Non-bias-limited tracking of spherical particles, enabling nanometer resolution at low magnification. *Biophys. J.*, **102**, 2362–2371.

34. Zhang,X.H., Chen,H., Fu,H.X., Doyle,P.S. and Yan,J. (2012) Two distinct overstretched DNA structures revealed by single-molecule thermodynamics measurements. *Proc. Natl. Acad. Sci. U.S.A.*, **109**, 8103–8108.

35. Ivani,I., Dans,P.D., Noy,A., Pérez,A., Faustino,I., Hospital,A., Walther,J., Andrio,P., Goñi,R. and Balaceanu,A. (2016) Parmbsc1: a refined force field for DNA simulations. *Nat. Methods*, **13**, 55–58.

36. Hess,B., Kutzner,C., Van Der Spoel,D. and Lindahl,E. (2008) GROMACS 4: algorithms for highly efficient, load-balanced, and scalable molecular simulation. *J. Chem. Theory Comput.*, **4**, 435–447.

37. Pérez,A., Marchán,I., Svozil,D., Sponer,J., Cheatham III,T.E., Laughton,C.A. and Orozco,M. (2007) Refinement of the AMBER force field for nucleic acids: improving the description of α/γ conformers. *Biophys. J.*, **92**, 3817–3829.

38. Jorgensen,W.L., Chandrasekhar,J., Madura,J.D., Impey,R.W. and Klein,M.L. (1983) Comparison of simple potential functions for simulating liquid water. *J. Chem. Phys.*, **79**, 926–935.

39. Carvalho,A.T., Gouveia,L., Kanna,C.R., Wärmländer,S.K., Platts,J.A. and Kamerlin,S.C.L. (2014) Understanding the structural and dynamic consequences of DNA epigenetic modifications: computational insights into cytosine methylation and hydroxymethylation. *Epigenetics*, **9**, 1604–1612.

40. Cieplak,P., Cornell,W.D., Bayly,C. and Kollman,P.A. (1995) Application of the multimolecule and multiconformational RESP methodology to biopolymers: charge derivation for DNA, RNA, and proteins. *J. Comput. Chem.*, **16**, 1357–1377.

41. Tan,Z.J. and Chen,S.J. (2006) Nucleic acid helix stability: effects of salt concentration, cation valence and size, and chain length. *Biophys. J.*, **90**, 1175–1190.

42. Xi,K., Wang,F.H., Xiong,G., Zhang,Z.L. and Tan,Z.J. (2018) Competitive binding of Mg2+ and na+ ions to nucleic acids: from helices to tertiary structures. *Biophys. J.*, **114**, 1776–1790.

43. Joung,I.S. and Cheatham III,T.E. (2008) Determination of alkali and halide monovalent ion parameters for use in explicitly solvated biomolecular simulations. *J. Phys. Chem. B*, **112**, 9020–9041.

44. Tan,Z.J. and Chen,S.J. (2007) RNA helix stability in mixed na+/mg2+ solution. *Biophys. J.*, **92**, 3615–3632.

45. Essmann,U., Perera,L., Berkowitz,M.L., Darden,T., Lee,H. and Pedersen,L.G. (1995) A smooth particle mesh ewald method. *J. Chem. Phys.*, **103**, 8577–8593.

46. Miyamoto,S. and Kollman,P.A. (1992) Settle: an analytical version of the SHAKE and RATTLE algorithm for rigid water models. *J. Comput. Chem.*, **13**, 952–962.

47. Martyna,G.J., Tobias,D.J. and Klein,M.L. (1994) Constant pressure molecular dynamics algorithms. *J. Chem. Phys.*, **101**, 4177–4189.

48. Van Der Spoel,D., Lindahl,E., Hess,B., Groenhof,G., Mark,A.E. and Berendsen,H.J. (2005) GROMACS: fast, flexible, and free. *J. Comput. Chem.*, **26**, 1701–1718.

49. Wu,Y.Y., Zhang,Z.L., Zhang,J.S., Zhu,X.L. and Tan,Z.J. (2015) Multivalent ion-mediated nucleic acid helix-helix interactions: RNA versus DNA. *Nucleic Acids Res.*, **43**, 6156–6165.

50. Bao,L., Zhang,X., Shi,Y.Z., Wu,Y.Y. and Tan,Z.J. (2017) Understanding the relative flexibility of RNA and DNA duplexes: stretching and twist-stretch coupling. *Biophys. J.*, **112**, 1094–1104.

51. Liu,J.H., Xi,K., Zhang,X., Bao,L., Zhang,X. and Tan,Z.J. (2019) Structural flexibility of DNA-RNA hybrid duplex: stretching and twist-stretch coupling. *Biophys. J.*, **117**, 74–86.

52. Bercovici,M., Han,C.M., Liao,J.C. and Santiago,J.G. (2012) Rapid hybridization of nucleic acids using isotachophoresis. *Proc. Natl. Acad. Sci. U.S.A.*, **109**, 11127–11132.

53. Kuhn,H., Demidov,V.V., Coull,J.M., Fiandaca,M.J., Gildea,B.D. and Frank-Kamenetskii,M.D. (2002) Hybridization of DNA and PNA molecular beacons to single-stranded and double-stranded DNA targets. *J. Am. Chem. Soc.*, **124**, 1097–1103.

54. Chen,C.L., Wang,W.J., Wang,Z., Wei,F. and Zhao,X.S. (2007) Influence of secondary structure on kinetics and reaction mechanism of DNA hybridization. *Nucleic Acids Res.*, **35**, 2875–2884.

55. Tawa,K. and Knoll,W. (2004) Mismatching base-pair dependence of the kinetics of DNA–DNA hybridization studied by surface plasmon fluorescence spectroscopy. *Nucleic Acids Res.*, **32**, 2372–2377.

56. Zacharias,M. (2020) Base-pairing and base-stacking contributions to double-stranded DNA formation. *J. Phys. Chem. B*, **124**, 10345–10352.

57. Friedman,R.A. and Honig,B. (1992) The electrostatic contribution to DNA base-stacking interactions. *Biopolymers*, **32**, 145–159.

58. Woodside,M.T., Behnke-Parks,W.M., Larizadeh,K., Travers,K., Herschlag,D. and Block,S.M. (2006) Nanomechanical measurements of the sequence-dependent folding landscapes of single nucleic acid hairpins. *Proc. Natl. Acad. Sci. U.S.A.*, **103**, 6190–6195.

59. Sabahi,A., Guidry,J., Inamati,G.B., Manoharan,M. and Wittung-Stafshede,P. (2001) Hybridization of 2 '-ribose modified mixed-sequence oligonucleotides: thermodynamic and kinetic studies. *Nucleic Acids Res.*, **29**, 2163–2170.

60. Shi,H., Liu,B., Nussbaumer,F., Rangadurai,A., Kreutz,C. and Al-Hashimi,H.M. (2019) NMR chemical exchange measurements reveal that N-6-Methyladenosine slows RNA annealing. *J. Am. Chem. Soc.*, **141**, 19988–19993.

61. Liu,B., Shi,H.L., Rangadurai,A., Nussbaumer,F., Chu,C.C., Erharter,K.A., Case,D.A., Kreutz,C. and Al-Hashimi,H.M. (2021) A quantitative model predicts how m(6)A reshapes the kinetic landscape of nucleic acid hybridization and conformational transitions. *Nat. Commun.*, **12**, 5201.

62. Sanstead,P.J., Ashwood,B., Dai,Q., He,C. and Tokmakoff,A. (2020) Oxidized derivatives of 5-Methylcytosine alter the stability and dehybridization dynamics of duplex DNA. *J. Phys. Chem. B*, **124**, 1160–1174.

63. Schwartz,J.J. and Quake,S.R. (2009) Single molecule measurement of the "speed limit" of DNA polymerase. *Proc. Natl. Acad. Sci. U.S.A.*, **106**, 20294–20299.

64. Muniz,L., Nicolas,E. and Trouche,D. (2021) RNA polymerase II speed: a key player in controlling and adapting transcriptome composition. *EMBO J.*, **40**, e105740.